Study on nonlinear multiaxial fatigue damage and reliability of TC4 titanium alloy for aeroengine blades

Bingqiang Li, Honggen Zhou, Jinfeng Liu, Chao Kang

School of Mechanical Engineering, Jiangsu University of Science and Technology, Zhenjiang, Jiangsu, 212003, P R China

Abstract

In order to study the fatigue damage and cycle life of TC4 titanium alloy for aero-engine blade under various load conditions, uniaxial fatigue, multi-stage loading and multiaxial fatigue tests were carried out on the titanium alloy sample. For uniaxial fatigue, the damage and life distribution of the alloy under different stress ratios and mean stresses were counted by axial fatigue test. In view of the shortcomings of the linear damage model, based on the Chaboche nonlinear damage model, the nonlinear damage evolution equation of TC4 titanium alloy was derived and the parameters were fitted. For multiple variable amplitude loadings, the calculation method of equivalent cycle number was deduced. The relationship between loading sequence and cumulative damage was studied. For multiaxial fatigue, the critical plane method combined with von Mises criterion was used to study the fatigue life distribution under various loading paths, and the results were verified by experiments. According to the simulation results of flow field of compressor blade under maximum continuous working condition, the stress time history of compressor blade was calculated. Based on the stress intensity interference model, the residual strength model of TC4 material was described. Combined with Poisson stochastic process, the reliability prediction of aero-engine compressor blade under maximum continuous working condition was completed. The results show that the fatigue damage and life distribution of TC4 titanium alloy for aeroengine blade under various conditions can be accurately predicted by the method proposed in this paper and the reliability of the blade can still be maintained above 0.9 after it works for 3000 hours under the maximum continuous working condition.

Keywords: TC4 alloy; Multiaxial damage; Fatigue life; Critical plane; Reliability

1. Introduction

Aeroengine is the heart of aircraft, and its material damage evolution mechanism directly determines its working life and reliability. The research on the influence of load parameters on the cumulative damage of materials can lay a foundation for the life prediction and design service life of the engine.

In fatigue damage analysis, Miner linear damage rule [1] is most commonly used. Considering that the cyclic loading is independent of each other and assuming that the material damage caused by the load cycle is independent of the load parameters, the damage value of the material is completely linear superposition during the service process in Miner model. In fact, the damage value is closely related to the load, and the cyclic stress amplitude lower than the fatigue limit will also cause damage to the material. The linear cumulative damage criterion is not applicable in the fatigue damage research of aero-engine parts, which will lead to more than three times over estimation [2].

Zhou et al. [3] used the improved equivalent strain model to predict the fatigue life of turbine blades. The applicability of the model was verified by a number of experimental data. Compared with SWT and morrow model, it showed that more accurate prediction results could be obtained by the model. Allegri et al. [4] used the nonlinear damage evolution model to study the fatigue crack initiation and propagation of materials. Considering the interaction of two horizontal stress loads, Gao et al. [5] proposed an improved nonlinear damage accumulation model. Experimental data of two metallic materials were adopted to validate the proposed model. The predicted values of the model were in good agreement with the experimental data, especially under high and low load conditions. Huffman et al. [6] presented a new phenomenological technique for using constant amplitude loading data to predict fatigue life. In the history of amplitude varying loading, damage was predicted by approximately cumulative damage from constant amplitude loading with a specific amplitude inversion strain range. Compared with other methods, the model proposed was verified by variable amplitude fatigue test data of three different

metals. Zuo et al. [7] applied nonlinear fatigue damage accumulation model to study the fatigue life prediction under variable amplitude load.

Considering the joint effect of high cycle fatigue and low cycle fatigue, Shao et al. [8] proposed a new fatigue reliability analysis method. Zhu et al. [9] predicted the fatigue life of turbine blade under the coupling effect of high cycle and low cycle fatigue. Oakley et al. [10] studied the high cycle and low cycle fatigue performance of turbine blades under the premise of damage of foreign objects. Hou et al. [11] predicted the fatigue cycle life of single crystal blade by using high and low cycle coupling fatigue model. Oller et al. [12] and Li et al. [13] studied the fatigue damage of mechanical structures under the combined action of heat and force. Song et al. [14] used fuzzy neural network algorithm to study the fatigue failure of disk system under fluid structure interaction. The method provided a useful idea for the optimization design of multi failure structure based on reliability, and enriched the theory and method of mechanical reliability design. Zhu et al [15] studied the influence of surface dent width depth ratio and other parameters on the ultra-high cycle fatigue properties of TC4 alloy.

On the basis of experiments, Chaboche et al. [16] established a nonlinear damage accumulation model, and proposed a damage evolution equation of the relationship between load parameters and material damage. Based on the work of Chaboche et al., many scholars had carried out fatigue life prediction and reliability research of mechanical structures [17-19]. At present, energy method [20,21], equivalent stress or strain method [22,23] and critical plane method [24] were three main methods to study multiaxial fatigue damage. Considering the phase difference between bending and torsion, Lee et al. [25] proposed an equivalent stress criterion under multi axial non-proportional loading.

Reliability is an important index to measure the quality of aero-engine. There are many methods to solve reliability, such as Petri net method [26], Monte Carlo method [27], artificial neural network method [28], Bayes method [29] and stress intensity interference method [30]. By extending the traditional stress intensity interference

theory, the reliability model of series system considering the statistical correlation between parts failure was established. Comparing with the prediction results of the traditional model, the superiority of the new model was proved [30]. In solving reliability problems, the stress strength interference method is the most suitable. Although the distribution of stress is difficult to express by mathematical formula, it can be solved by finite element method.

In this paper, the fatigue test of TC4 alloy was carried out. In view of the deficiency of linear model to describe material damage, the nonlinear model describing damage calculation and life prediction of TC4 alloy is described by combining the Chaboche nonlinear damage criterion and multiaxial fatigue theory, and the parameters were fitted according to the test results. The classical Wöhler curve method and BP neural network method [31] are introduced to calculate the life distribution of samples, and the accuracy of the model is proved by comparing with the test results. For multistage load, the calculation method of equivalent cycle number is derived in this paper. The relationship between damage accumulation and residual strength of TC4 material and load parameters is further developed. A nonlinear residual strength model is established, and a time-varying reliability model of blade is established by introducing Poisson stochastic process. According to the flow field simulation and finite element calculation results, the reliability of the blade in the maximum continuous working state is reasonably predicted.

2 Nonlinear damage model

2.1 Determination of cumulative damage

Caused by cyclic loading fatigue damage, the static strength of the material decreases with time, which can be expressed as [32]:

$$F_r = F_{r0}(1-D)^{\frac{r+\alpha_0+1}{r}} \tag{1}$$

where F_r, F_{r0} and D are the residual strength, initial strength and cumulative damage of the material, respectively. Both r and α_0 are material parameters. For titanium alloy, α_0 is 0 and the value of r is between 10 and 15, which can be determined by looking up the table or testing. The cumulative damage can be calculated by measuring the

static strength with this method.

In the symmetrical tension compression (R =-1) fatigue test for TC4 alloy, taking the dimensionless cycle ratio as the abscissa, the damage values of material are calculated using Miner linear cumulative damage criterion and compared with test results, as are shown in Fig. 1, where n is the number of load cycles and N_f is the cycle life. Without containing the information of load, Miner linear criterion shows a straight line in any case. The test results show that the residual strength is still higher than 50% of the initial strength after the first 80% stress cycle damage, and then during 20% of the cycle residual strength drops sharply and the damage increases significantly. The higher the stress amplitude, the greater the damage increase rate. Obviously, Miner linear damage criterion is difficult to accurately describe the cumulative damage of TC4 alloy due to its inability to express load information.

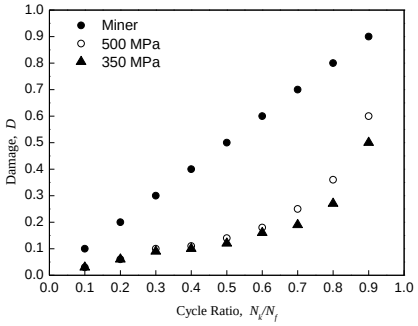

Fig.1 Damage for TC4 alloy (R=-1)

2.2 Chaboche multiaxial nonlinear damage model

Due to the large error of the linear damage model, Chaboche proposed the following general nonlinear model [16]:

$$\mathrm{d}D = f(D,\sigma)\mathrm{d}n \tag{2}$$

where σ is a load parameter. For uniaxial fatigue damage problem, Chaboche derived the concrete expression form as:

$$\mathrm{d}D=\left[1-(1-D)^{1+\beta}\right]^{\alpha}\left[\frac{\sigma_a}{M(1-b\sigma_m)(1-D)}\right]^{\beta}\mathrm{d}n \tag{3}$$

where σ_a is the amplitude of stress cycle, σ_m is the mean stress, M, β and b are the parameters related to material, and α is a parameter related to the load, which can be described as:

$$\alpha=1-\frac{1}{H}\langle\sigma\rangle=1-\frac{1}{H}\left\langle\frac{\sigma_{\max}-\sigma_{\mathrm{f}}}{\sigma_{\mathrm{b}}-\sigma_{\max}}\right\rangle^{h} \tag{4}$$

where H and h are the parameters related to material, σ_b and σ_f are tensile strength and fatigue limit, respectively. σ_{max} is maximum stress value，and $\langle x\rangle=\begin{cases}0, x\le 0\\ x, x>0\end{cases}$.

Considering the characteristics of aero-engine and the complex aerodynamic excitation working environment, the cumulative damage of torsional vibration is very important. In this paper, the multiaxial damage research of materials is carried out based on the critical plane method. Fig. 2 shows the tension and torsion diagram of the specimen, where x-axis and z-axis are the axial line and outer normal direction of the specimen, respectively. Setting the critical plane rotates around z axis at the angle of θ first and then around the x axis at the angle of ϕ, then in the x-y-z coordinate system, one may obtain:

$$\boldsymbol{\varepsilon}'_{\mathrm{NP}}=\mathbf{M}^{\mathrm{T}}\boldsymbol{\varepsilon}_{\mathrm{NP}}\mathbf{M} \tag{5}$$

where

$$\boldsymbol{\varepsilon}_{\mathrm{NP}}=\begin{bmatrix}\varepsilon_{xx}^{\mathrm{NP}} & \frac{1}{2}\gamma_{xy}^{\mathrm{NP}} & 0\\ \frac{1}{2}\gamma_{xy}^{\mathrm{NP}} & -\nu\varepsilon_{xx}^{\mathrm{NP}} & 0\\ 0 & 0 & -\nu\varepsilon_{xx}^{\mathrm{NP}}\end{bmatrix} \tag{6}$$

$$\mathbf{M}=\begin{bmatrix}\cos\theta & -\sin\theta\cos\phi & \sin\theta\sin\phi\\ \sin\theta & \cos\theta\cos\phi & -\cos\theta\sin\phi\\ 0 & \sin\phi & \cos\phi\end{bmatrix} \tag{7}$$

Under the condition of non-proportional loading, if the applied strain load is in the form of sine wave and the phase difference is φ, that is:

$$\varepsilon_{xx}^{\mathrm{NP}} = \varepsilon_{xx}\sin\omega t$$
$$\gamma_{xy}^{\mathrm{NP}} = \lambda\varepsilon_{xx}\sin\left(\omega t-\varphi\right) \tag{8}$$

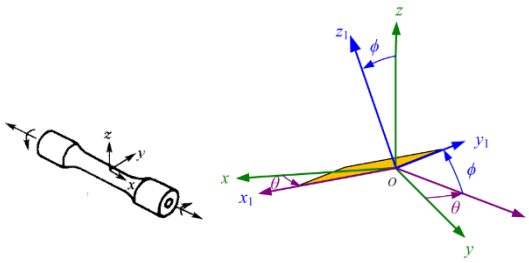

Fig.2 Diagram of tension and torsion of specimen

When $\sigma_{xy}^2 > \sigma_{xx}\sigma_{yy}$, The critical plane is perpendicular to the free plane, let ϕ=90° , the shear strain and normal strain are obtained as follows:

$$\gamma = (\varepsilon_{xx})_a\{[(1+\nu)\,sin\,2\,\theta - \lambda\,cos\,2\,\theta\,cos\,\varphi]^2 + [\lambda\,cos\,2\,\theta\,sin\,\varphi]^2\}^{1/2}\,sin(\omega t+\beta_1) \tag{9}$$

$$\varepsilon = \frac{(\varepsilon_{xx})_a}{2}\{[2(1+\nu)\,cos^2\,\theta + \lambda\,sin\,2\,\theta\,cos\,\varphi - 2\nu]^2 + [\lambda\,sin\,2\,\theta\,sin\,\varphi]^2\}^{1/2}\,sin(\omega t+\beta_3) \tag{10}$$

where

$$\beta_1 = tan^{-1}\{\lambda\,cos\,2\,\theta\,sin\,\varphi\,/[(1+\nu)\,sin\,2\,\theta - \lambda\,cos\,2\,\theta\,cos\,\varphi]\} \tag{11}$$

$$\beta_3 = tan^{-1}\{\lambda\,sin\,2\,\theta\,sin\,\varphi\,/[(1+\nu)(1-cos\,2\,\theta) - \lambda\,sin\,2\,\theta\,cos\,\varphi - 2\nu]\} \tag{12}$$

Let $\frac{\partial\gamma}{\partial\theta}=0$, the orientation angle of the critical plane is obtained as:

$$\theta_{\mathrm{cp}} = \frac{1}{4}\tan^{-1}\left\{2\lambda(1+\nu)\cos\varphi/[(1+\nu)^2-\lambda^2]\right\} \tag{13}$$

Then we can get:

$$\gamma_{\max} = \gamma\left(\theta_{\mathrm{cp}}\right),\ \varepsilon_n = \varepsilon_{\max}\left(\theta_{\mathrm{cp}}\right) \tag{14}$$

Using Von Mises criterion to synthesize the equivalent strain by two parameters on the critical plane, it can be obtained that:

$$\frac{\Delta\varepsilon_{eq}}{2} = \left[\left(\Delta\varepsilon_n/2\right)^2 + \frac{1}{3}\left(\Delta\gamma_{\max}/2\right)^2\right]^{1/2} \tag{15}$$

The equivalent stress can be expressed as:

$$\frac{\Delta\varepsilon_{eq}}{2}=\eta\frac{\sigma_{eq}}{E} \tag{16}$$

where

$$\eta=\begin{cases}1, & \sigma_{\max}\le\sigma_y\\ \sigma_{\max}/\sigma_y, & \sigma_{\max}>\sigma_y\end{cases} \tag{17}$$

Substituting Eq. (15) into Eq. (3), yields:

$$\mathrm{d}D=\left[1-(1-D)^{1+\beta}\right]^{\alpha}\left[\frac{\eta E\left[\left(\frac{\Delta\varepsilon_n}{2}\right)^2+\frac{1}{3}(\Delta\gamma_{max}/2)^2\right]^{1/2}}{M(1-b\sigma_m)(1-D)}\right]^{\beta}\mathrm{d}n \tag{18}$$

According to Von Mises theory, mean stress σ_{m} under multiaxial loading condition can be calculated as:

$$\sigma_m=(\sigma_n^2+3\sigma_t^2)^{\frac{1}{2}} \tag{19}$$

where σ_n and σ_t denote average normal stress and shear stress, respectively. Through the integration, the fatigue life prediction expression under any load level can be obtained as follows:

$$N_f=\frac{1}{1-\alpha}\frac{1}{1+\beta}\left[\frac{M(1-b\sigma_m)}{\eta E\left[\left(\frac{\Delta\varepsilon_n}{2}\right)^2+\frac{1}{3}(\Delta\gamma_{max}/2)^2\right]^{1/2}}\right]^{\beta} \tag{20}$$

Under constant amplitude excitation, after n-th loading cycles, the damage value is:

$$D=1-\left\{1-\left[n(1-\alpha)(1+\beta)\left[\frac{M(1-b\sigma_m)}{\eta E\left[\left(\frac{\Delta\varepsilon_n}{2}\right)^2+\frac{1}{3}(\Delta\gamma_{max}/2)^2\right]^{1/2}}\right]^{-\beta}\right]^{\frac{1}{1-\alpha}}\right\}^{\frac{1}{1+\beta}} \tag{21}$$

3 Fatigue test and discussion

3.1 Uniaxial fatigue test

The fatigue specimens of TC4 alloy are provided by Northwest institute of nonferrous metals, and have been treated by hydrogen dehydrogenation. The dimensions are shown in Fig. 3. The main chemical compositions and tensile properties of TC4 alloy are shown in Tab. 1 and Tab. 2, respectively.

Tab. 1 Composition of TC4 alloy （ω/%）

Ti	Al	V	Fe	Zr	Mn	Mo	Sn	Nb	Pd
88.16	5.18	3.91	0.15	0.10	0.10	0.50	0.50	0.50	0.19

Tab. 2 Tensile properties of TC4 alloy

Parameter	Value
Young's modulus *E*/GPa	1.14
Possion ratio *v*	0.3
Density ρ/g/cm^3	4.4
Yield strength σ_y/MPa	975
Tensile strength σ_b/Mpa	1005

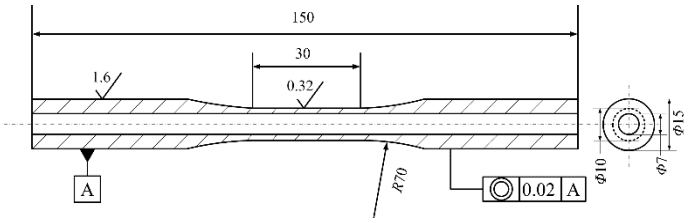

Fig. 3 TC4 alloy fatigue specimen

Firstly, uniaxial fatigue test is carried out. The Instron 8874 axial torsion high frequency fatigue testing machine is used, and the sampling frequency is set as 130 Hz. Two kinds of stress ratio are selected to carry out fatigue test, namely symmetrical tension compression test with R =-1 and pull-up test with R= 0.1. The stress of the first sample is set as 0.6-0.7 times of the tensile strength, and the maximum stress of the second sample is 0.5-0.6 times of the tensile strength. The stress levels are reduced successively until the number exceeds reference cycles (10^7). In the up and down method, setting a number of stress levels, if the previous sample fails to complete the reference cycles (10^7), the stress level will be reduced. If the previous test piece goes out, the stress level will be increased.

Some typical data are selected. The pull-up test results with R = 0.1 is shown in Tab. 3 while the symmetrical tension and compression test results with R =-1 are shown in Fig. 4. Summing up the data in Tab. 3 and Fig. 4, it can be seen that the fatigue life gradually decreases with the increase of stress level. The stress amplitude directly determines the average life, and the mean stress has a great influence on the cycle life. For example, for No.5 sample (R = 0.1), the average stress is 396.5MPa while the stress amplitude is about 320MPa, and the life is 1.96 million cycles. In the test with R =-1, the life of the sample with stress amplitude of 320MPa is about 8.2 million

cycles.

Tab. 3 Axial fatigue test results (R=0.1)

Serial Number	Maximum Stress/MPa	Fatigue life/10^4Cycle
1	596.7	1002.8
2	632.1	1002.8
3	667.5	1000.3
4	702.9	217.4
5	716.5	196.9
6	730.9	52.3
7	745.3	44.5
8	759.7	38.1
9	774.1	6.7
10	738.7	48.1

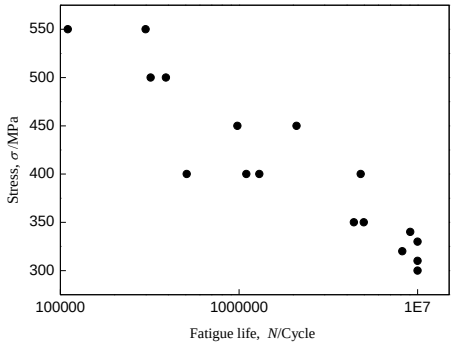

Fig.4 Axial fatigue test results (R=-1)

The material parameters of TC4 alloy are obtained by fitting the test data, as shown in Tab. 4.

Tab. 4 Parameter values of TC4 alloy

M	h	H	β	b	σ_f'	ξ
1.86×10^{10}	0.434	0.081	0.757	0.0029	1835.35	-0.099

The classical three-layer BP neural network is selected to predict the fatigue life of the alloy, as shown in Fig. 5, in which the number of hidden layer neurons is set as 10, and L-M algorithm is selected to train the network. The algorithm has the advantage of fast convergence speed and can avoid the modification of Hessian matrix to the network. The modification of L-M algorithm to Hessian matrix is as follows:

$$x(k+1) = x(k) - \left[J^T J + \mu I \right]^{-1} J^T e \tag{22}$$

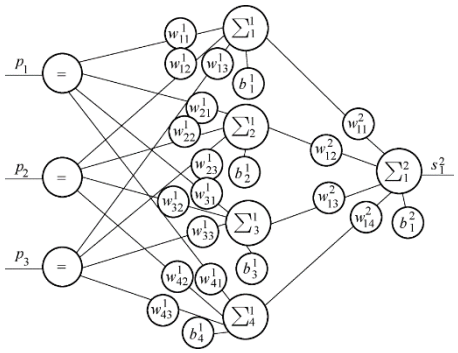

Fig. 5 Three-layer BP neural network

Since the Wöhler curve method can not consider the average stress value, the working condition of R =-1 is selected to carry out the comparison between the calculation results of the three methods and the test results, as shown in Fig. 6.

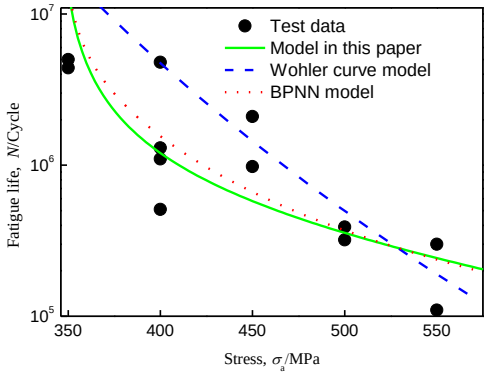

Fig. 6 Comparison of fatigue life prediction (R=-1)

It can be seen from Fig. 6 that the accuracy degree of Wöhler model is low, while the accuracy of nonlinear damage model in this paper and BP neural network model is higher. Compared with the model in this paper, the calculation process of BP neural network model is more complex and there is no explicit physical expression.

Taking the experimental data with R=-1 as the sample, the damage values predicted by the damage evolution equation are compared with the test results under three cyclic stress levels of 350Mpa, 400MPa and 500MPa, as shown in Fig. 7. It can be seen that the accuracy of the model in this paper is very high.

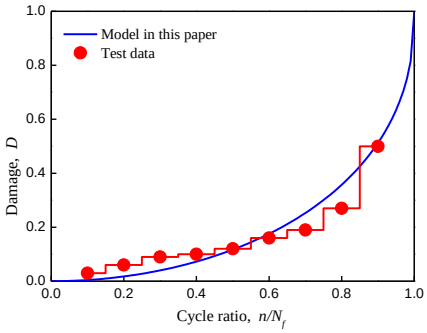

(a) 350MPa

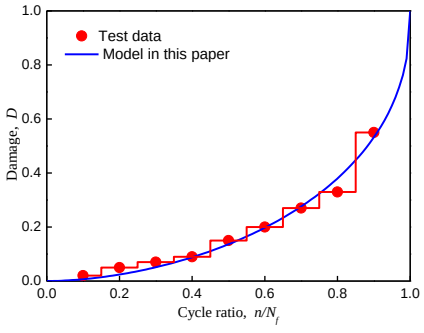

(b) 400MPa

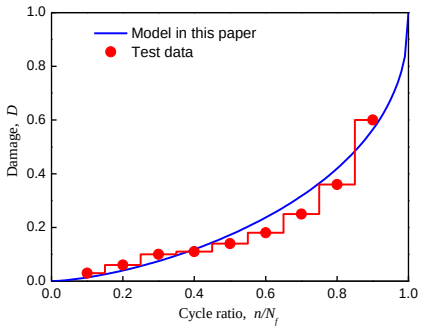

(c) 500MPa

Fig. 7 Comparison between damage prediction results and experiment data under different stress levels (R=-1)

3.2 Multistage loading test

Under multi-stage load excitation, when the specimen undergoes n_1 cycles at the stress amplitude σ_{a1}, and then fails after n_2 cycles at the stress amplitude σ_{a2}. If the cyclic life of the specimen under the stress amplitude σ_{a1} is N_{f1}, and the cyclic life of the specimen under the stress amplitude σ_{a2} is N_{f2}, N_2 is defined as the equivalent number of cycles under the stress level σ_{a2} reaching the same damage value as n_1 cycles under the stress amplitude σ_{a1}, then:

$$1-\left[1-\left(\frac{n_1}{N_{f1}}\right)^{1/(1-\alpha_1)}\right]^{1/(1+\beta)}=1-\left[1-\left(\frac{N_2}{N_{f2}}\right)^{1/(1-\alpha_2)}\right]^{1/(1+\beta)}\Rightarrow\frac{N_2}{N_{f2}}=\left(\frac{n_1}{N_{f1}}\right)^{(1-\alpha_2)/(1-\alpha_1)} \tag{23}$$

The relationship between n_2 and n_1 is obtained as follows:

$$\frac{n_2}{N_{f2}}=1-\frac{N_2}{N_{f2}}\Rightarrow\frac{n_2}{N_{f2}}=1-\left(\frac{n_1}{N_{f1}}\right)^{(1-\alpha_2)/(1-\alpha_1)} \tag{24}$$

The two-stage load fatigue tests are carried out under three working conditions of 350-500 MPa, 400-500

MPa and 350-400 MPa, respectively (R=-1). When the stress amplitudes are loaded in the order of first high and then low, the expression is as follows:

$$\frac{1-\alpha_2}{1-\alpha_1}<1 \Rightarrow \frac{n_2}{N_{f2}}+\frac{n_1}{N_{f1}}<1 \tag{25}$$

That is, the sum of horizontal and vertical coordinate values is less than 1, and vice versa. The experimental results are in good agreement with the predicted data under the excitation of two-level loading, as shown in Fig. 8, which verifies the accuracy of the model in this paper.

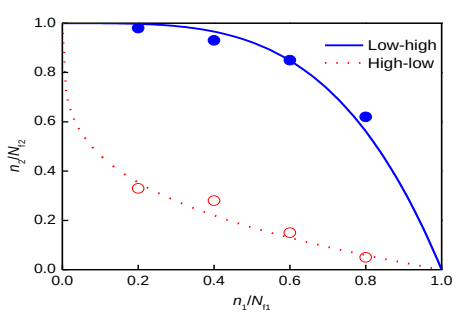

(a) 350-500 MPa

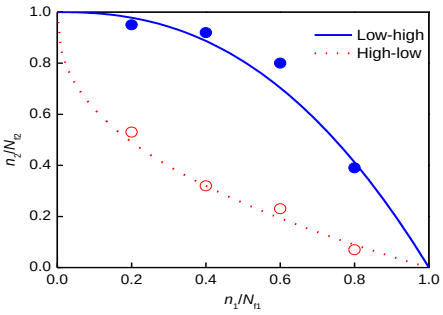

(b) 400-500 MPa

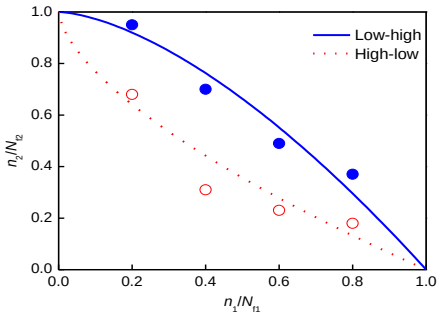

(c) 350-400MPa

Fig. 8 Cycle ration distribution curves under two-level loading (R=-1)

3.3 Multiaxial fatigue test

Multiaxial fatigue tests are carried out under proportional loading and four non-proportional loading conditions. The time domain waveforms of five kinds of loadings are shown in Fig. 9 (a), while the loading path and the strain distribution in the cross section are shown in Fig. 9 (b) and (c), respectively. Under each loading path, 10 samples are tested with different stress amplitudes. The comparison between the calculated results and the

experimental results is shown in Fig. 10. It can be seen from that the error is the smallest under proportional loading condition; when the phase difference is smaller, the calculation accuracy is higher; while the phase difference is at the same value, the closer the loading amplitudes along the two shafts are, the more accurate the life prediction is. Generally speaking, the life prediction accuracy of the specimens under five loading paths is relatively good.

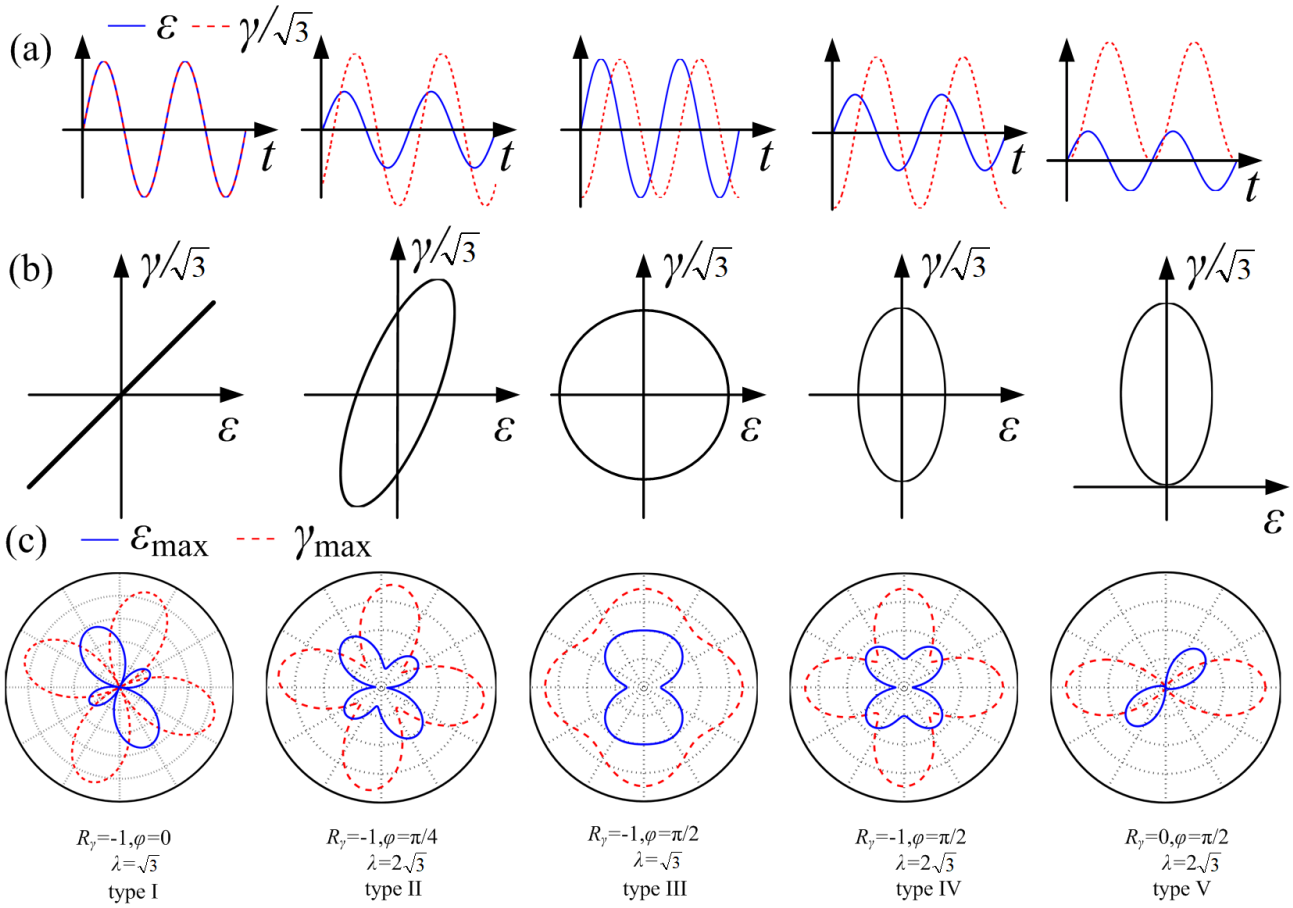

Fig. 9 Multiaxial fatigue test: (a) waveform of multiaxial loading, (b) loading path, (c) strain distribution

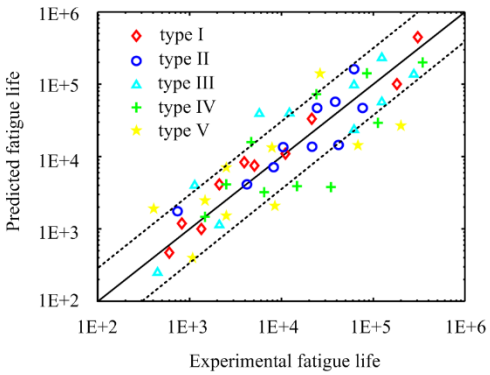

Fig. 10 Comparison between the calculated results and the experimental results

4 Dynamic simulation of compressor blade

According to the compressor rotor system of an aeroengine, the three-dimensional geometric model and three-dimensional flow field model are established. The influence of stator wake is considered by using sliding grid and the input of the previous stage stator pressure. The rotating speed of the aeroengine in the maximum continuous working state is that ω=11383 rpm, and the fluid medium is air. The total pressure at the stator inlet is that P_{inlet}=1.0 atm and total temperature T_{inlet}=300 K (under standard atmospheric pressure condition); the static pressure at the outlet is that P_{outlet}=1.08 atm while the total temperature T_{outlet}=300 K. The Mach number at inlet position is 0.07 under the condition of compressible flow field. The specific boundary conditions are shown in Fig. 11.

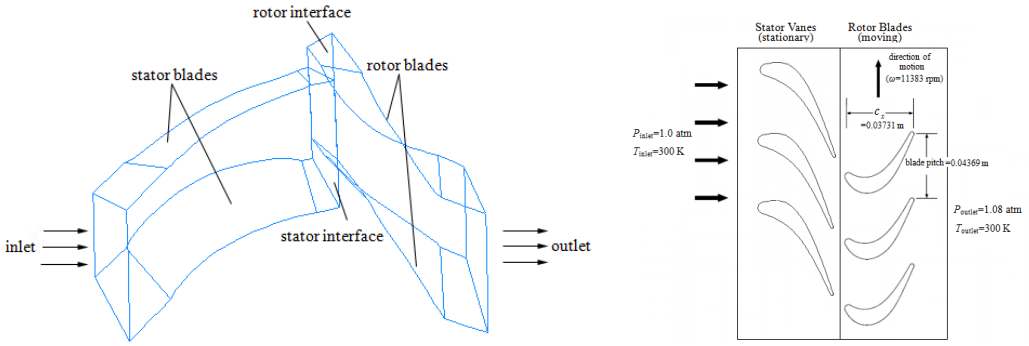

(a) Three-dimensional single sector flow field channel's boundary (b) Two-dimensional flow field boundary condition

Fig. 11 Description of compressor flow field

The three-dimensional flow field of the former stage stationary blade and the downstream moving blade are taken as the research objects for calculation of aerodynamic loadings. The number of moving and stationary blades is equal, both 38. The structure model and flow field model are shown in Fig. 11. The single sector flow field channel is selected as the calculation area, and the structured hexahedron mesh is generated by Gambit, a professional preprocessing tool of commercial CFD software. The total number of grid elements is 106758, of which the number of elements in moving blade flow field area is 31046, and that of stationary blade flow field area is 75712. After checking, the length width ratio of the grid is less than 5, and the quality of the grid is good, as shown in Fig. 12.

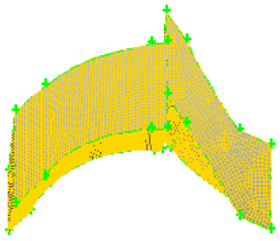

Fig. 12 Gambit model of single sector flow field

The periodic flow field model is generated by Fluent, as shown in Fig. 13.

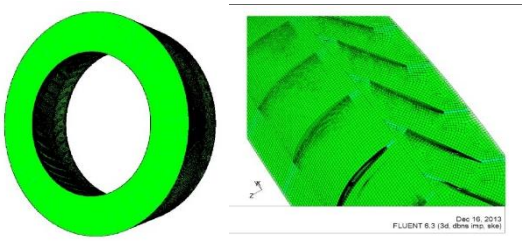

Fig. 13 Fluent periodical model of flow field

The solution method is set as implicit coupling solution and 500 step steady analysis is carried out firstly. Then, the steady flow field is used as the initial field for unsteady analysis. The physical time step is defined as T/60, where T is the period of dynamic and static interference. The number of virtual iteration steps is set to 20, and the calculation time step is 2280. After the convergence of iterative calculation results, the aerodynamic load distribution on suction surface and pressure surface of blade presents periodic changes, and the peak load results are shown in Fig. 14.

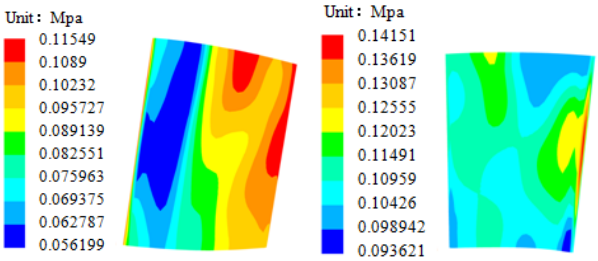

(a) Pressure surface (b) Suction surface

Fig.14 Aerodynamic peak load of compressor blades

MSC Nastran software is used to solve the dynamic problem in time domain by local stress-strain method, and the solution time and time step are set as 1s and 10^4, respectively. Considering the coupling effect of compression and torsion for blades, the maximum normal strain and maximum shear strain at each node are extracted and the equivalent stress is synthesized according to Eqs. (15)-(17). The calculation results show that the maximum equivalent stress point is located in the middle of the convex side of the blade, which is 5-6 mm away from the root. The time history of strain

is shown in Fig. 15.

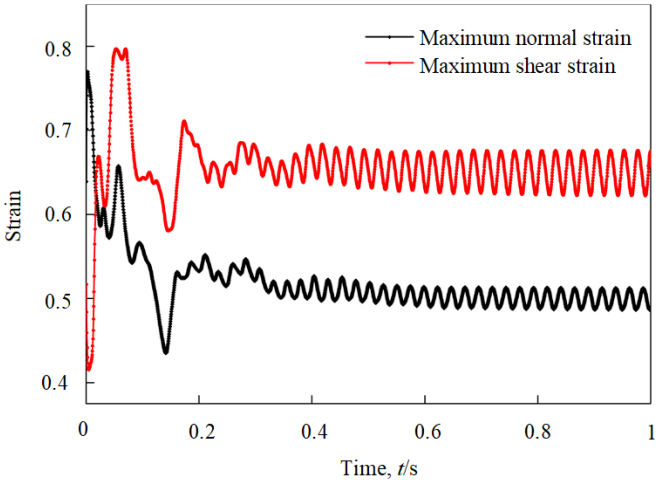

Fig. 15 Time domain history of strain

5 Reliability calculation of blade

The stress strength interference model can be expressed as follows:

$$R = P(r > s) = \int_{-\infty}^{+\infty} f_s(s) \int_{s}^{+\infty} f_r(r)\, \mathrm{d}r\mathrm{d}s \tag{26}$$

where $f_r(r)$ is the probability density function of the structure strength and $f_s(s)$ is the probability density function of the stress. The model is based on the independence of stress and strength without considering the relationship between strength degradation and load cycle.

In the actual working process, the strength degradation is a function of load. When the number of load cycles is n, the probability of that no failure occurs is given by:

$$R(n) = \prod_{i=1}^{n} R_i = \prod_{i=1}^{n} \int_{0}^{\infty} f_s(s) \int_{s}^{\infty} f_r(r,s,i)\, \mathrm{d}r\mathrm{d}s \tag{27}$$

where $f_r(r,s,i)$ is the probability density function of strength for blades during the i-th cycle.

According to Eq. (1) and Eq. (21), the residual strength can be described as follows:

$$r(n) = F_{r0}\left\{1 - \left[n(1-\alpha)(1+\beta)\left[\frac{M(1-b\sigma_m)}{\eta E\left[\left(\frac{\Delta\varepsilon_n}{2}\right)^2 + \frac{1}{3}(\Delta\gamma_{max}/2)^2\right]^{1/2}}\right]^{-\beta}\right]^{\frac{1}{1-\alpha}}\right\}^{\frac{1}{1+\beta}\frac{r+1}{r}} \tag{28}$$

where $r(n)$ represents the residual strength after n-th load cycles.

A Poisson process with strength λ is used to describe the counting of the number of cycles. The reliability of the blade at the moment $t + \Delta t$ can be expressed as:

$$R(t+\Delta t)=R(t)\left\{\sum_{x=0}^{\infty}P(n=x)[1-\lambda\Delta t+\lambda\Delta tP(r(x)>s)]\right\}=R(t)\left\{\sum_{x=0}^{\infty}P(n=x)[1-\lambda\Delta t+\lambda\Delta tF_s r(n)]\right\} \tag{29}$$

When Δt is small enough, Eq. (29) is transformed into the form of differential equation as:

$$\frac{\mathrm{d}R(t)}{R(t)\mathrm{d}t}=\frac{R(t+\Delta t)-R(t)}{R(t)\Delta t}=-\lambda e^{-t}\sum_{x=0}^{\infty}\frac{t^x}{x!}[1-F_s r(n)] \tag{30}$$

By solving the differential equation, the reliability expression of blade at time t is obtained as follows:

$$R(t)=exp\left\{-\int_0^t\lambda e^{-\lambda}\sum_{x=0}^{\infty}\frac{\lambda^x}{x!}\left\{1-F_sF_{r0}\left\{1-\left[n(1-\alpha)(1+\beta)\left[\frac{M(1-b\sigma_m)}{\eta E\left[\left(\frac{\Delta\varepsilon_n}{2}\right)^2+\frac{1}{3}(\Delta\gamma_{max}/2)^2\right]^{1/2}}\right]^{-\beta}\right]^{\frac{1}{1-\alpha}}\right\}^{\frac{1}{1+\beta}\frac{r+1}{r}}\right\}dt\right\} \tag{31}$$

The time-varying reliability is calculated by the time-domain stress history of the blade under the maximum continuous working condition. The damage and residual strength are calculated in terms of the number of cycles, which are transformed into corresponding time distributions. The calculation results of TC4 blade reliability distribution under this condition are shown in Fig. 16.

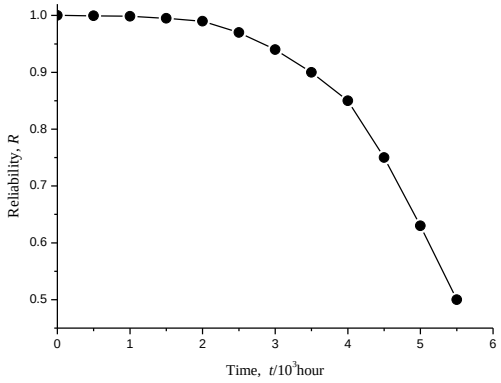

Fig. 16 Calculation results of reliability distribution of blades

According to the calculation results, the reliability of the blade has been maintained above 0.9 within 3000 hours. After 4000 hours, the reliability decreases rapidly, to 5500 hours, the reliability is close to 0.5.

6 Conclusions

In this paper, the nonlinear multiaxial fatigue damage and reliability of TC4 titanium alloy for Aeroengine

blades are studied, and some conclusions can be drawn as follows:

(1) The fatigue life distribution of TC4 alloy specimens under symmetric cycle of R =-1 and asymmetric cycle of R=0.1 were obtained by experiments. When the cycle ratio was taken as the abscissa, the damage variable shows highly nonlinear.

(2) Under the condition of uniaxial fatigue test, the parameters of Chaboche nonlinear cumulative damage model are fitted, and the accuracy of this model is verified to be higher than other models by comparing with the test results.

(3) For multi-stage variable amplitude loadings, the calculation method of equivalent cycle number is derived, and the relationship between loading sequence and cumulative damage is studied and verified by test.

(4) For multiaxial fatigue, the error is the smallest under proportional loading condition; when the phase difference is smaller, the calculation accuracy is higher; while the phase difference is at the same value, the closer the loading amplitudes along the two shafts are, the more accurate the life prediction is. Generally speaking, the life prediction accuracy of the specimens under five loading paths is relatively good.

(5) Based on the stress intensity interference model and Poisson stochastic process, the time-varying reliability function with strength degradation is established. The calculation results show that the reliability can still be maintained above 0.9 when the blade works for 3000 hours at the maximum continuous working state.

References

[1] Miner M A. Cumulative damage in fatigue [J]. Applied Mechanics, 1945, 67(12): 59-64

[2] Fatemi A, Yang L X. Cumulative fatigue damage and life prediction theories: a survey of the state of the art for homogeneous materials [J]. International Journal of Fatigue, 1998, 20(1): 9-34

[3] Zhou J , Huang H Z , Peng Z . Fatigue life prediction of turbine blades based on a modified equivalent strain model [J]. Journal of Mechanical Science and Technology, 2017, 31(9):4203-4213

[4] Allegri G , Wisnom M R . A non-linear damage evolution model for mode II fatigue delamination onset and growth [J]. International Journal of Fatigue, 2012, 43:226-234

[5] Gao H , Zuo F , Huang H Z , et al. A modified non-linear damage accumulation model considering load interaction effects under two-level loading [C]. China, International Conference on Quality, 2013, 1774

[6] Huffman P J , Beckman S P . A non-linear damage accumulation fatigue model for predicting strain life at variable amplitude loadings based on constant amplitude fatigue data [J]. International Journal of Fatigue, 2013, 48:165-169

[7] Zuo F J, Huang H Z, Zhu S P, et al. Fatigue life prediction under variable amplitude loading using a non-linear damage accumulation model [J]. International Journal of Damage Mechanics, 2014, 0(0): 1-18.

[8] Shao X J, Cao L J, Liu G S, et al. A new kind of reliability analysis method in coupled case of high-cycle fatigue and low-cycle fatigue [C]. China, International Conference on Quality, 2012, 966

[9] Zhu S P , Yue P , Yu Z Y , et al. A Combined High and Low Cycle Fatigue Model for Life Prediction of Turbine Blades [J]. Materials, 2017, 10(7):1-15

[10] Oakley S Y , Nowell D. Prediction of the combined high- and low-cycle fatigue performance of gas turbine blades after foreign object damage [J]. International Journal of Fatigue, 2007, 29(1): 69-80

[11] Hou N X , Wen Z X , Yu Q M, et al. Application of a combined high and low cycle fatigue life model on life prediction of SC blade [J]. International Journal of Fatigue, 2009, 31(4):616-619

[12] Oller S, Salomón O, Onate E. A continuum mechanics model for mechanical fatigue analysis [J]. Computational Materials Science, 2005, 32(2):175-195

[13] Li L B. In-phase thermomechanical fatigue damage evolution of long fiber-reinforced ceramic-matrix composites using fatigue hysteresis-based damage parameters [J]. International Journal of Mechanical Sciences, 2018: S0020740317331119

[14] Song L, Wen J, Fei C, et al. Distributed collaborative probabilistic design of multi-failure structure with fluid-structure interaction using fuzzy neural network of regression [J]. Mechanical Systems and Signal Processing, 2018, 104:72-86

[15] Zhu L N , Deng C Y , Wang D P , et al. Effect of surface roughness on very high cycle fatigue behavior of Ti-6Al-4V alloy[J].

Acta Metallurgica Sinica, 2016, 52(5):583-591

[16] Chaboche J L, Lesne PM. A non-linear continuous fatigue damage model [J]. Fatigue and fracture of engineering materials and structures, 1988, 11(1): 1-17

[17] Dattoma V , Giancane S , Nobile R , et al. Fatigue life prediction under variable loading based on a new non-linear continuum damage mechanics model [J]. International Journal of Fatigue, 2006, 28(2):89-95

[18] Lin J W, Zhang J H, Yang S, et al. Reliability analysis of aero-engine blades considering nonlinear strength degeneration [J]. Chinese Journal of Aeronautics, 2013, 26(3):631-637

[19] Karolczuk A, Skibicki D, Pejkowski, L. Evaluation of the fatemi-socie damage parameter for the fatigue life calculation with application of the Chaboche plastic model[J]. Fatigue and fracture of engineering materials and structures, 2018:1-12

[20] Park J, Nelson D. Evaluation of an energy-based approach and a critical plane approach for predicting constant amplitude multiaxial fatigue life[J]. International journal of fatigue, 2000, 22(1): 23-39

[21] Djebli A, Aid A, Bendouba M, et al. A non-linear energy model of fatigue damage accumulation and its verification for Al-2024 aluminum alloy [J]. International Journal of Non-Linear Mechanics, 2013, 51:145-151

[22] Lazzarin P, Susmel L. A stress based method to predict lifetime under multi-axial fatigue loadings [J]. Fatigue and fracture of engineering materials and structures, 2003, 26(12): 1171-1187

[23] Aid A , Bendouba M , Aminallah L , et al. An equivalent stress process for fatigue life estimation under multiaxial loadings based on a new non-linear damage model[J]. Materials Science and Engineering A, 2012, 538:20-27

[24] Fatemi A, Socie D F. A critical plane approach to multi-axial fatigue damage including out of phase loading [J]. Fatigue and fracture of engineering materials and structures, 1988, 11(3): 149-165

[25] Lee S B. A criterion for fully reversed out-of-phase torsion and bending [J]. American Society for Testing and Materials, 1985, 553-568

[26] Kabir S, Papadopoulos Y. Applications of Bayesian networks and Petri nets in safety, reliability, and risk assessments: A review[J]. Safety Science, 2019, 115:154-175

[27] Liu K, Wu J, Liu H, et al. Reliability analysis of thermal error model based on DBN and Monte Carlo method[J]. Mechanical Systems and Signal Processing, 2021, 146:107020

[28] Izquierdo J, Crespo Marquez A, Uribetxebarria J. Dynamic Artificial Neural Network-based reliability considering operational context of assets[J]. Reliability Engineering and System Safety, 2019, 188(8):483-493

[29] Yin M X, Zhu T, Xu J T, et al. Service reliability of a heavy-haul wagon coupler body based on the SMOTE-Bootstrap-Bayes method[J]. Engineering Failure Analysis, 2020, 118

[30] Yan Y. Load characteristic analysis and fatigue reliability prediction of wind turbine gear transmission system[J]. International Journal of Fatigue, 2020, 130(1):105259.1-105259.9

[31] Cadoso J B, Almeida J R, Dias J M, et al. Structural reliability analysis using Monte Carlo simulation and neural networks [J]. Advances in Engineering Software, 2008, 39(6): 505-513

[32] Gu Y W, An W G, An H. Structural Reliability Analysis Under Dead Load and Fatigue Load [J]. Acta Armamentarii, 2017, 28(12): 1473-1477